

How To Make A Thesis Following The Guideline With More Text To Have Two Lines



by

A Good Name

Submitted for the degree of

Doctor of Philosophy

SOME WEIRD INSTITUTE NO ONE EVER HEARD ABOUT

SCHOOL OF LATEX AND WRITING

HERIOT-WATT UNIVERSITY

September 2042

Abstract

In accordance with the Academic Regulations the thesis must contain an abstract preferably not exceeding 200 words, bound in to precede the thesis. The abstract should appear on its own, on a single page. The format should be the same as that of the main text. The abstract should provide a synopsis of the thesis and shall state clearly the nature and scope of the research undertaken and of the contribution made to the knowledge of the subject treated. There should be a brief statement of the method of investigation where appropriate, an outline of the major divisions or principal arguments of the work and a summary of any conclusions reached. The abstract must follow the Title Page.

Dedication

If a dedication is included then it should be immediately after the Abstract page.

I don't what it is actually.

Acknowledgements

I wanna thanks all coffee and tea manufacturers and sellers that made the completion of this work possible.

Contents

I	Chapters	1
1	Introduction	2
1.1	Paragraph: Introduction to Stellite Alloys for Hostile Environments IG-NORE_HEADING	2
1.2	Role of HIPping vs as Cast	2
1.3	Paragraph: Tungsten and Molybdenum carbides	2
1.4	Corrosion resistance of Stellites	6
2	Analytical Investigations	8
2.1	Strain hardening	8
2.2	Correlative empirical methods	8
3	Experimental Investigations	11
3.1	Materials and Microstructure	11
3.2	Materials and Microstructure	11
3.3	Experimental determination of SFE	12
3.4	Electrochemical instrument and experiments	13
3.5	Stellite 1	15
3.6	Stellites	15
3.7	Objectives and Scope of the Research Work	15
3.8	Thesis Outline	15
3.9	Literature Survey	15
3.10	Cavitation Tests	15
4	Discussion	16
4.1	Experimental Test Procedure	16
4.1.1	Hardness Tests	16
4.1.2	Cavitation	16
4.2	Relationships between cavitation erosion resistance and mechanical properties . .	16
4.3	Influence of vibratory amplitude	16
	References	17

List of Tables

List of Figures

Glossary

BSE Backscatter Electrons.

EDX Energy-Dispersive X-ray.

FCC Face Centred Cubic.

HCP Hexagonal Close Packed.

HIP Hot Isostatically Pressed.

HV Hardness Vickers Scale.

PDF Powder Diffraction File.

SE Secondary Electrons.

SEM Scanning Electron Microscope/Microscopy.

XRD X-ray Diffraction.

Part I

Chapters

Chapter 1

Introduction

1.1 Paragraph: Introduction to Stellite Alloys for Hostile Environments

IG-

NORE_HEADING

Stellites are a family of cobalt-base superalloys used in aggressive service environments due to retention of strength, wear resistance, and oxidation resistance at high temperature [1, 2]. Starting with Elwood Haynes's development of alloys like Stellite 6 in the early 1900s [3], stellites became critical to components used in medical implants & tools, machine tools, and nuclear components, and new variations on the original CoCrWC and CoCrMoC alloys see expanding use in sectors like oil & gas and chemical processing [1, 4, 5].

The main alloying elements in Stellite alloys are cobalt (Co), chromium (25-33 wt% Cr), tungsten (0-18 wt% W), molybdenum (0-18 wt% Mo), carbon (0.1-3.3 wt% C), and trace elements iron (Fe), nickel (Ni), silicon (Si), phosphorus (P), sulphur (S), boron (B), lanthanum (La), & manganese (Mn); Table 1.3 summarizes the nominal and measured composition of commonly used Stellite alloys [6–15]. Stellite alloys possess a composite-like microstructure, combining a cobalt-rich matrix strengthened by solid solutions of chromium, tungsten, & molybdenum, with embedded hard carbide phases with carbide formers Cr (of carbide type M_7C_3 & $M_{23}C_6$) and W/Mo (of carbide type MC & M_6C), that impede wear and crack propagation [16, 17].

1.2 Role of HIPping vs as Cast

1.3 Paragraph: Tungsten and Molybdenum carbides

Tungsten (W) and molybdenum (Mo) are refractory elements that provide solid solution strengthening to the matrix, by virtue of their large atomic size that impedes dislocation flow when present as solute atoms [18], and also form M_6C and $M_{12}C$ carbides along with MC carbides and Co_3M & Co_7M_6 intermetallics during solidification.

In carbon-rich regions, the MC phase (of type WC and MoC) is observed [19], which ca

In carbon-poor regions, ternary M_6C and $M_{12}C$ carbides have been identified, where the M_6C carbide (of type Co_3Mo_3C) is stable in the temperature ranges of 900C to 1300C and can vary in composition from $Mo_{40}Co_{46}C_{14}$ to $Mo_{56}Co_{30}C_{14}$, while the $Mo_{12}C$ carbide of type (Co_6Mo_6C

Alloy	Co	Cr	W	Mo	C	Fe	Ni	Si	P	S	B	La	Mn	Ref	Process	Type	Observation
Stellite 1	47.7	30	13	0.5	2.5	3	1.5	1.3					0.5	[10]			Nominal composition
	48.6	33	12.5	0	2.5	1	1	1.3					0.1	[7]			
	46.84	31.7	12.7	0.29	2.47	2.3	2.38	1.06					0.26	[6]	HIPed ^a		ICP-OES ^b
Stellite 3	50.5	33	14		2.5									[9]			
	49.24	29.57	12.07	0.67	2.52	2.32	1.07	1.79					0.75	[14]	HIPed ^a		ICP-OES ^b
Stellite 4	45.43	30	14	1	0.57	3	3	2					1	[10]			Nominal composition
	51.5	30	14		1	1	2	0.5						[15]			
	51.9	33	14		1.1									[9]			
	49.41	31	14	0.12	0.67	2.16	1.82	1.04					0.26	[6]	HIPed ^a		ICP-OES ^b
	50.2	29.8	14.4	0	0.7	1.9	1.9	0.8					0.3	[8]	HIPed ^a		
Stellite 6	51.5	28.5	4.5	1.5	1	5	3	2			1		2	[10]			Nominal composition
	63.81	27.08	5.01		0.96	0.73	0.87	1.47					0.07	[14]	HIPed ^a		ICP-OES ^b
	60.3	29	4.5		1.2	2	2	1						[15]			
	61.7	27.5	4.5	0.5	1.15	1.5	1.5	1.15					0.5	[9]			
	58.46	29.5	4.6	0.22	1.09	2.09	2.45	1.32					0.27	[6]	HIPed ^a		ICP-OES ^b
	58.04	30.59	4.72		1.24	2.03	1.87	0.80	0.01	0.01				[12]	PTAW ^c		OES
	55.95	27.85	3.29		0.87	6.24	3.63	1.23	0.01	0.01			0.45	[12]	GTAW ^d		OES
	52.40	30.37	3.57		0.96	6.46	3.93	1.70	0.01	0.01			0.3	[12]	SMAW ^c		OES

	60.3		31.10	4.70	0.30	1.10	1.70	1.50	1.30	0.00	0.3	[13]	LP-DED	ICP-AES & GDMS
	60.6	27.7	5	0	1.2	1.9	2	1.3			0.3	[8]	HIPed ^a	
Stellite 12	53.6	30	8.3		1.4	3	1.5	0.7			1.5	[10]		Nominal composition
	55.22	29.65	8.15	0.2	1.49	2.07	2.04	0.91			0.27	[6]	HIPed ^a	ICP-OES ^b
Stellite 19	50.94	31.42	10.08	0.79	2.36	1.82	2	0.4		0.09	0.1	[11]		
Stellite 20	41.05	33	17.5		2.45	2.5	2.5				1	[10]		Nominal composition
	43.19	31.85	16.3	0.27	2.35	2.5	2.28	1			0.26	[6]	HIPed ^a	ICP-OES ^b
Stellite 21	59.493	27		5.5	0.25	3	2.75	1		0.007	1	[10]		Nominal composition
	60.6	26.9	0	5.7	0.2	1.3	2.7	1.9			0.7	[8]	HIPed ^a	
Stellite 31	57.5	22	7.5		0.5	1.5	10	0.5			0.5	[10]		Nominal composition
	52.9	25.3	7.8	0	0.5	1.1	11.4	0.6			0.4	[8]	HIPed ^a	
Stellite 190	46.7	27	14	1	3.3	3	3	1			1	[10]		Nominal composition
	48.72	27.25	14.4	0.2	3.21	2.1	2.81	1			0.31	[6]	HIPed ^a	ICP-OES ^b

carbide decomposes into Mo_6C and $\mu - Mo$ phases above 1100C [20].

When present in large quantities, W and Mo also participate in formation of W-rich or Mo-rich carbides during alloy solidification [5, 10],

leading to generation of Topologically Close-Packed (TCP) phases, such as the μ phase (of type Co_7W_6 and Co_7Mo_6) and σ phase (pf type Co_3W and Co_3Mo) [19], which are intermetallic brittle phases that add strength to the material [21, 22] while also promoting crack initiation and propagation [23]. Previous work on the Stellite 1 sample by Ahmed et al [6] indicate that Co_6W_6C is identified as the main W-rich carbide in Stellite 1, although Co_3W_3C was also identified in addition to Co_3W and Co_7W intermetallics.

There are two main phases in the tungsten-carbon system: the hexagonal monocarbide WC (ICDD Card# 03-065-4539, COD:2102265), denoted as $\delta - WC$, and multiple variations of hexagonal-close-packed subcarbide W_2C (ICDD:00-002-1134, COD:1539792) [24, 25]

WC carbides precipitate as discrete particles distributed heterogeneously throughout the alloy intragranularly

The precipitation of the tungsten-rich phase M_6C is closely related to the decomposition of the MC carbide, and the M_6C only occurs in the vicinity of the MC [26], as M_6C carbides form only when the tungsten and/or molybdenum content exceeds 4-6 a/o.

Chromium carbides have high hardness and wear resistance, as well as excellent resistance to chemical corrosion, making them often used in surface coatings [27]

In the Cr-C binary phase diagram, there are three phases : cubic $Cr_{23}C_6$ (space group , melting point 1848 K), orthorhombic Cr_3C_2 (space group Pnma, melting point 2083 K) and Cr_7C_3 (space group Pnma, melting point 2038 K) [28] [27]

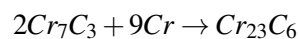
The $M_{23}C_6$ carbides are formed during heat treatment of carbides with a lower M/C ratio or from solid solution close to boundaries [28]. Fine $M_{23}C_6$ carbides act as obstacles to gliding of mobile dislocations, which result in long-term creep strength [29].

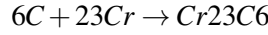
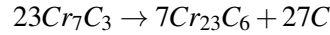
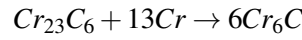
Although $M_{23}C_6$ can precipitate as primary carbide during solidification, it is most commonly found in secondary carbides along grain boundaries.

M_7C_3 is a metastable pseudo-eutectic carbide that typically forms at lower carbon-chromium ratios and effectively transforms into secondary $M_{23}C_6$ upon heat treatment.

In addition to being a carbide former, chromium provides solid solution strengthening and corrosion/oxidation resistance to the cobalt-based matrix.

The Cr_7C_3 carbide is unstable at high temperatures and transforms to $M_{23}C_6$ upon heat treatment. Under further temperature and time, $Cr_{23}C_6$ partially transforms to Cr_6C [30].





The remarkable ability of Stellite alloys to withstand these specific challenges stems from key metallurgical features. Their corrosion resistance is primarily attributed to a high chromium content, typically 20-30 wt.%, which promotes the formation of a highly stable, tenacious, and self-healing chromium-rich passive oxide film on the material's surface; this film acts as a barrier isolating the underlying alloy from the corrosive environment. Alloying elements such as molybdenum and tungsten can further enhance this passivity, particularly improving resistance to localized corrosion phenomena like pitting and crevice corrosion in aggressive media. Concurrently, their outstanding cavitation resistance is largely derived from the unique behavior of the cobalt-rich matrix, which can undergo a stress-induced crystallographic transformation from a face-centered cubic (fcc) to a hexagonal close-packed (hcp) structure. This transformation, often facilitated by mechanical twinning, effectively absorbs the intense, localized impact energy from collapsing cavitation bubbles and leads to significant work hardening, thereby impeding material detachment and erosion.

Antony suggests that the cavitation-erosion resistance of Stellites derives from the matrix phase and is enhanced by the strain-induced fcc \rightarrow hcp allotropic transformation [31].

1.4 Corrosion resistance of Stellites

The cavitation erosion of stellites has been investigated in experimental studies [Wang2023, Szala2022741, Mitelea2022967, Liu2022, Sun2021, Szala2021, Zhang2021, Mutascu2019776, Kovalenko2019175, E201890, Ciubotariu2016154, Singh201487, Hattori2014257, Depczynski20131045, Singh2012498, Romo201216, Hattori20091954, Ding201797, Guo2016123, Ciubotariu201698], along with investigations into cobalt-based alloys [Lavigne2022, Hou2020, Liu2019, Zhang20191060, E2019246, Romero2019581, Romero2019518, Lei20119, Qin2011209, Ding200866, Feng2006558].

Stellites achieve oxidation resistance through the formation of a passivating external Cr₂O₃ scale, due to the high proportion of Cr in their chemical composition [32].

as seen by Zhang et al in Green Death solution [33].

However, Cr-based carbides may be preferentially oxidized below the external Cr₂O₃ scale, particularly at the boundary of carbides which are depleted of Cr [33], where preferential attack of carbides proceed until they have been consumed [32].

Lemaire et al [34] investigated the behavior of Stellite 6 in pressurized high temperature water and proposed an oxidative wear mechanism where wear proceeds by repeated detachment of the surface oxide spontaneously forming on the stellite surface.

Di Martino et al [35] also found that the protective chromium-rich film are abraded easily, leading to further corrosion.

In such lower-temperature regimes, the passive films formed are typically very thin (in the nanometer range, rather than the micrometer scale observed at high temperatures)

Molybdenum and tungsten have favorable effects on the selective oxidation of chromium until chromium has been depleted, at which point molybdenum and tungsten result in increased oxidation due to development of less protective phases [32].

Chapter 2

Analytical Investigations

2.1 Strain hardening

Cavitation bubble collapse induce a work hardening of the material surface, comparable to that obtained in conventional peening [36], characterized by the thickness of the hardened layers and the shape of the strain profile below the surface.

The strain profile within the material can usually be modeled by the following power law:

$$\varepsilon(x) = \varepsilon_s \left(1 - \frac{x}{L}\right)^\theta \quad (2.1)$$

where $\varepsilon(x)$ is the strain at depth x from the eroded surface, ε_s is the failure rupture strain on the eroded surface, L is the thickness of the hardened layer, and θ is the shape factor of the power law.

After each cycle, the thickness of the hardened layer L and the surface strain ε_s will increase continuously until damage is initiated at the surface (ε_s reaches the failure rupture strain ε_R), at which point the strain profile is in steady-state.

$$\varepsilon_R = \varepsilon_{mean} \left(1 - \frac{\Delta L}{L + \Delta L}\right)^\theta \quad (2.2)$$

In Woodford's investigations on the $\gamma\delta\epsilon$ transformation on the surface of cobalt-base alloys during cavitation erosion, the transformed layer was found to extend to a depth of 25 to 50

¹Converted from the original 1e-3 to 2e-3 [37]].

2.2 Correlative empirical methods

Empirical methods are common for addressing complex cavitation erosion, involving lab tests to correlate cavitation erosion resistance with mechanical properties.

1. Karimi and Leo

The Karimi and Leo phenomenological model describes cavitation erosion rate as a function of

Karimi and Leo

2. Noskievic

Noskievic formulated a mathematical relaxation model for the dynamics of the cavitation erosion using a differential equation applied to forced oscillations with damping:

$$\frac{d^2v}{dt^2} + 2\alpha \frac{dv}{dt} + \beta^2 v = I \quad (2.3)$$

where I is erosion intensity, which can vary linearly with time, $v = \frac{dv}{dt}$ is erosion rate, α is strain hardening or internal friction of material during plastic deformation, and β is coefficient inversely proportional to material strength. The general solution of equation can be written as:

$$v = af_0(\delta, \tau) + bf_1(\delta, \tau) \quad (2.4)$$

$$f_0(\delta, \tau) = \begin{cases} 1 - \exp(-\delta\tau) \left[\frac{\delta}{\omega} \sin(\omega\tau) + \cos(\omega\tau) \right] & \text{if } -1 < \delta < 1; \delta \neq 0 \\ 1 - \frac{1}{\delta_0^2 - 1} \left[\delta_0^2 \exp\left(-\frac{\tau}{\delta_0}\right) - \exp(-\delta_0\tau) \right] & \text{if } \delta > 1 \\ 1 - \cos(\tau) & \text{if } \delta = 0 \\ 1 - (1 + \tau) \exp(-\tau) & \text{if } \delta = 1 \end{cases} \quad (2.5)$$

$$f_1(\delta, \tau) = \begin{cases} 1 - \frac{2\delta}{\tau} [1 - \exp(-\delta\tau) [\cos\omega\tau + \varepsilon \sin\omega\tau]] & \text{if } -1 < \delta < 1; \delta \neq 0 \\ 1 - \frac{1}{\tau} \left(2\delta - \frac{1}{\delta_0(\delta_0^2 - 1)} \left[\exp(-\delta_0\tau) - \delta^4 \exp\left(\frac{-\tau}{\delta_0}\right) \right] \right) & \text{if } \delta > 1 \\ 1 - \frac{\sin(\tau)}{\tau} & \text{if } \delta = 0 \\ 1 - \frac{2[1 - \exp(-\tau)]}{\tau} + \exp(-\tau) & \text{if } \delta = 1 \end{cases} \quad (2.6)$$

$$\delta = \frac{\alpha}{\beta}, \quad \tau = \beta t, \quad \varepsilon = \frac{\delta^2 - 0.5}{\delta \sqrt{1 - \delta^2}}, \quad \omega = \sqrt{1 - \delta^2}, \quad \delta_0 = \delta + \sqrt{\delta^2 - 1} \quad (2.7)$$

3. Hoff and Langbein equation

Hoff and Langbein proposed a simple exponential function for the rate of erosion, representing the normalized erosion rate requiring only the A simple exponential function for the rate of erosion was proposed by Hoff and Langbein,

$$\frac{\dot{e}}{e_{\max}} = 1 - e^{-\frac{t_i}{\tau}}$$

\dot{e} - erosion rate at any time t e_{max} - Maximum of peak erosion rate t_i - incubation period
(intercept on time axis extended from linear portion of erosion-time curve) t - exposure time

4. L Sitnik model

$$V = V_o \left[\ln \left(\frac{t}{t_o} + 1 \right) \right]^\beta$$

$$\dot{V} = \frac{\beta V_o}{t + t_o} \left[\ln \left(\frac{t}{t_o} + 1 \right) \right]^{\beta-1}$$

$$V_o > 0 \quad t_o > 0 \quad \beta \geq 1$$

Chapter 3

Experimental Investigations

3.1 Materials and Microstructure

The HIPed Stellite 1 alloys were manufactured by canning the gas-atomized powders, manufactured by Deloro Stellite (UK), at a temperature and pressure of 1200C and 100 MPa, for 4 hours in a HIPing vessel where the chemical composition and sieve analysis have been reported in previous work by Ahmed et al [38].

The sieve analysis of these powders indicate that the majority of powder particles were in the size range of 45 to 180 μm .

The cast alloy samples were produced via sand casting process.

	Co	Cr	W	Mo	C	Fe	Ni	Si	Mn
HIPed Stellite 1	Bal.	31.70	12.70	0.29	2.47	2.30	2.38	1.06	0.26
			+250	+180	+125	+45	-45		
HIPed Stellite 1		0.10	2.40	47.90	49.50	0.10			

3.2 Materials and Microstructure

The HIPed alloy was produced via canning the gas-atomized powders at 1200C and 100 MPa pressure for 4h, while the cast alloys were produced via sand casting. % Sieve analysis and description of powders

% Refer to Table of chemical compositions of both cast and HIPed alloys.

The microstructure of the alloys were observed via SEM in BSE mode, and the chemical compositions of the identified phases developed in the alloys were determined via EDS as well as with XRD under $\text{Cu } K_{\alpha}$ radiation.

Image analysis was also conducted to ascertain the volume fractions of individual phases.

The Vickers microhardness was measured using a Wilson hardness tester under loads of BLAH. Thirty measurements under each load were conducted on each sample.

The microstructure phase identification was investigated out using X-ray diffraction technique with $\text{Cu-K}\alpha$ radiation ($\lambda = 1.5406$). The volume fraction of ϵ -Co can be determined using the

intensity of the $(200)_\gamma$ and $(10\bar{1}1)_{hcp}$ peaks, using the following equation proposed by Sage and Guillaud:

$$\text{hcp}(\text{vol}\%) = \frac{I(10\bar{1}1)_\epsilon}{I(10\bar{1}1)_\epsilon + 1.5I(200)_\gamma} \quad (3.1)$$

3.3 Experimental determination of SFE

To experimentally determine the SFE, the XRD method proposed by Reed and Schramm was employed [39]:

$$SFE = \frac{K_{111}\omega_0 G_{111}a_0}{\pi\sqrt{3}} \frac{\langle \epsilon_{50}^2 \rangle_{111}}{\alpha} A^{-0.37} \quad (3.2)$$

where:

$$K_{111}\omega_0 = 6.6G_{111} = \frac{1}{3} \frac{1}{C_{44} + C_{11} - C_{12}} A = \frac{1C_{44}}{C_{11} - C_{12}} \quad (3.3)$$

ployed [39]:

SFE = stacking fault energy $\frac{mJ}{m^2}$ $K_{111}\omega_0 = 6.6$, as obtained by A is the Zener elastic anisotropy C_{ij} are elastic stiffness coefficients G_{111} is the shear modulus of the (111) -plane, in which stacking faults are formed a_0 is the lattice constant of the fcc-metal matrix $\langle \epsilon_{111}^2 \rangle_{50}$ is the root mean square microstrain in the $\langle 111 \rangle$ direction averaged over the distance of 50 α is stacking fault probability

1. Elastic constant

Microhardness measurements were taken on the surfaces of the as-cast and HIPed samples. The Wilson Tukon 1102 hardness tester was used for Vickers microhardness testing with a load of 300 grams ($HV_{0.3}$) for 10s, and averaged by using ten individual indentations. The specimen surface was prepared in the same fashion as for microstructural analysis.

Previous work

The indentation fracture toughness was made with hardness equipment (AVK-A, AKASHI) at a load of 49 N for 10 s, and the value was obtained from five measurements on the cross section. The fracture toughness was evaluated based to the Evans-Wilshaw equation [21, 22].

$$K_{IC} = 0.079 \left(\frac{P}{a^{\frac{3}{2}}} \right) \log \left(\frac{4.5a}{c} \right) \quad (3.4)$$

where P is indenter load [mN], $2c$ is the crack length [μm], and $2a$ is the length of indentation diagonal [μm]

3.4 Electrochemical instrument and experiments

A Corrtest potentiostat was used for electrochemical experiments in a conventional three electrode cell, with the sample as working electrode with exposed area 2cm², a saturated calomel electrode (SCE) as reference electrode, and a Pt plate as counterelectrode.

All electrochemical experiments were performed at room temperature.

The open circuit potential was continuously recorded for 1 h, before the electrical impedance spectroscopy (EIS), LPR, and cyclic voltametry experiments.

The aqueous oxidation of Stellite 6 alloy was investigated in a 1979 study using X-ray Photoelectron Spectroscopy (XPS) [40]. Specimens were exposed to pH 10 water at 285°C. To understand the oxidation behavior, the study measured dissolved oxygen concentration against exposure duration.

The high-temperature corrosion resistance of stellite coatings is attributable to the formation of cobalt & chromium surface [41].

Heathcock et al found that carbides are selectively eroded, with the carbide-matrix interface acting as initiating erosion site [42].

1. Paragraph 4: Synergistic Challenges in Applications Prone to Corrosion and Cavitation
IGNORE

2. Paragraph 5: Research and Development for Enhanced Corrosion and Cavitation Performance
IGNORE

3. Paragraph 6: Influence of HIPing
IGNORE

Compared with the case alloys, the HIPed alloys had relatively finer, rounded, and distributed carbides.

4. Paragraph: Cavitation Erosion Resistance

The primary result of an erosion test is the cumulative mass loss versus time, which is then converted to volumetric loss and mean depth of erosion (MDE) versus time for the purposes of comparison between materials of different densities. The calculation of the mean depth of erosion for this test method should be performed in conformity with ASTM G-32.

5. General Background %cite:@Franc2004265, @Romo201216, @Kumar2024, @Kim200685, @Gao2024, @20221xix, @Usta2023, @Cheng2023, @Zheng2022

Cavitation erosion presents a significant challenge in materials degradation in various industrial sectors, including hydroelectric power, marine propulsion, and nuclear systems,

stemming from a complex interaction between fluid dynamics and material response [43, 44]. Hydrodynamically, the phenomenon initiates with the formation and subsequent violent collapse of vapor bubbles within a liquid, triggered by local pressures dropping to the saturated vapor pressure. These implosions generate intense, localized shockwaves and high-speed microjets that repeatedly impact adjacent solid surfaces [45]. From a materials perspective, these impacts induce high stresses (100-1000 MPa) and high strain rates, surpassing material thresholds and leading to damage accumulation via plastic deformation, work hardening, fatigue crack initiation and propagation, and eventual material detachment. Mitigating this requires materials capable of effectively absorbing or resisting this dynamic loading, often under demanding conditions that may also include corrosion.

% Martensitic transformation Crucially, the cobalt matrix often possesses a low stacking fault energy, facilitating a strain-induced martensitic transformation from a metastable face-centered cubic γ phase to a hexagonal close-packed ϵ phase under the intense loading of cavitation. This transformation is a primary mechanism for dissipating impact energy and enhancing work hardening, contributing significantly to Stellite's characteristic cavitation resistance [46, 47].

HIPing is a thermo-mechanical material processing technique which involves the simultaneous application of pressure (up to 200 MPa) and temperature (2000 C), which results in casting densification, porosity closure, and metallurgical bonding. [48]

While commonly applied via casting or weld overlays, processing routes like Hot Isostatic Pressing (HIP) offer potential advantages such as microstructure refinement [49] finer microstructures and enhanced fatigue resistance [48, 50].

HIPing of surface coatings results in microstructure refinement, which can yield improved fatigue and fracture resistance.

HIPing leads to carbide refinement, which can yield improved impact toughness [51], and reduce carbide brittleness [48].

Furthermore, HIP facilitates the consolidation of novel 'blended' alloys created from mixed elemental or pre-alloyed powders, providing a pathway to potentially tailor compositions or microstructures for optimized performance. However, despite the prevalence of Stellite alloys and the known influence of processing on microstructure and properties, the specific cavitation erosion behavior of HIP-consolidated Stellites, particularly these blended formulations, remains underexplored in academic literature. Given that erosion mechanisms in Stellites often involve interactions at the carbide-matrix interface [52], understanding how HIP processing and compositional blending affect these interfaces and the matrix's transformative capacity under cavitation, especially when potentially coupled with corrosion,

constitutes a critical knowledge gap addressed by this research.

% Need to describe Stellite 1

3.5 Stellite 1

Stellite 1 is a high-carbon and high-tungsten alloy, making it suitable for demanding applications that require hardness & toughness to combat sliding & abrasive wear [[17](#)]

3.6 Stellites

3.7 Objectives and Scope of the Research Work

3.8 Thesis Outline

3.9 Literature Survey

3.10 Cavitation Tests

Chapter 4

Discussion

4.1 Experimental Test Procedure

4.1.1 Hardness Tests

4.1.2 Cavitation

4.2 Relationships between cavitation erosion resistance and mechanical properties

4.3 Influence of vibratory amplitude

% Insert the whole spiel by that French dude about displacement and pressure (and then ruin it) The pressure of the solution depends on the amplitude of the vibratory tip attached to the ultrasonic device. Under simple assumptions, kinetic energy of cavitation is proportional to the square of the amplitude and maximum hammer pressure is proportional to A.

$$x = A \sin(2\pi ft) \quad (4.1)$$

$$v = \frac{dx}{dt} = 2\pi f A \cos(2\pi ft) \quad (4.2)$$

$$v_{max} = 2\pi f A \quad (4.3)$$

$$v_{mean} = \frac{1}{\pi} \int_0^\pi A \sin(2\pi ft) = 4fA \quad (4.4)$$

$$(4.5)$$

However, several researchers have found that erosion rates are not proportional to the second power of amplitude, but instead a smaller number. Thiruvengadam [53] and Hobbs find that erosion rates are proportional to the 1.8 and 1.5 power of peak-to-peak amplitude. Tomlinson et al find that erosion rate is linearly proportional to peak-to-peak amplitude in copper [3]. Maximum erosion rate is approximately proportional to the 1.5 power of p-p amplitude [4]. The propagation of ultrasonic waves may result in thermal energy absorption or into chemical energy, resulting in reduced power. For the purposes of converting data from studies that do not use an amplitude of 50um, a exponent factor of 1.5 has been applied.

References

- [1] R. Ahmed, H. L. de Villiers Lovelock, N. H. Faisal, and S. Davies, "Structure–property relationships in a CoCrMo alloy at micro and nano-scales," *Tribology International*, vol. 80, pp. 98–114, Dec. 1, 2014, ISSN: 0301-679X. DOI: [10.1016/j.triboint.2014.06.015](https://doi.org/10.1016/j.triboint.2014.06.015). Accessed: Jun. 30, 2024. [Online]. Available: <https://www.sciencedirect.com/science/article/pii/S0301679X14002436>.
- [2] J.-C. Shin, J.-M. Doh, J.-K. Yoon, D.-Y. Lee, and J.-S. Kim, "Effect of molybdenum on the microstructure and wear resistance of cobalt-base Stellite hardfacing alloys," *Surface and Coatings Technology*, vol. 166, no. 2, pp. 117–126, Mar. 24, 2003, ISSN: 0257-8972. DOI: [10.1016/S0257-8972\(02\)00853-8](https://doi.org/10.1016/S0257-8972(02)00853-8). Accessed: Mar. 5, 2025. [Online]. Available: <https://www.sciencedirect.com/science/article/pii/S0257897202008538>.
- [3] M. S. Hasan, A. M. Mazid, and R. Clegg, "The Basics of Stellites in Machining Perspective," *International Journal of Engineering Materials and Manufacture*, vol. 1, no. 2, pp. 35–50, Dec. 19, 2016, ISSN: 0128-1852. DOI: [10.26776/ijemm.01.02.2016.01](https://doi.org/10.26776/ijemm.01.02.2016.01). Accessed: May 11, 2025. [Online]. Available: <https://deerhillpublishing.com/index.php/ijemm/article/view/13>.
- [4] U. Malayoglu and A. Neville, "Comparing the performance of HIPed and Cast Stellite 6 alloy in liquid–solid slurries," *Wear*, 14th International Conference on Wear of Materials, vol. 255, no. 1, pp. 181–194, Aug. 1, 2003, ISSN: 0043-1648. DOI: [10.1016/S0043-1648\(03\)00287-4](https://doi.org/10.1016/S0043-1648(03)00287-4). Accessed: Feb. 17, 2025. [Online]. Available: <https://www.sciencedirect.com/science/article/pii/S0043164803002874>.
- [5] D. Raghu and J. B. C. Wu, "Recent Developments in Wear and Corrosion Resistant Alloys for Oil Industry," presented at the CORROSION 1997, Association for Materials Protection and Performance, Mar. 9, 1997, pp. 1–20. DOI: [10.5006/C1997-97016](https://doi.org/10.5006/C1997-97016). Accessed: May 12, 2025. [Online]. Available: <https://dx.doi.org/10.5006/C1997-97016>.
- [6] R. Ahmed, A. Fardan, and S. Davies, "Mapping the mechanical properties of cobalt-based stellite alloys manufactured via blending," *Advances in Materials and Processing Technologies*, vol. 0, no. 0, pp. 1–30, Jun. 2, 2023, ISSN: 2374-068X. DOI: [10.1080/2374068X.2023.2220242](https://doi.org/10.1080/2374068X.2023.2220242). Accessed: Jul. 13, 2024. [Online]. Available: <https://doi.org/10.1080/2374068X.2023.2220242>.

- [7] M. Alimardani, V. Fallah, A. Khajepour, and E. Toyserkani, "The effect of localized dynamic surface preheating in laser cladding of Stellite 1," *Surface and Coatings Technology*, vol. 204, no. 23, pp. 3911–3919, Aug. 25, 2010, ISSN: 0257-8972. DOI: [10.1016/j.surfcoat.2010.05.009](https://doi.org/10.1016/j.surfcoat.2010.05.009). Accessed: Mar. 31, 2025. [Online]. Available: <https://www.sciencedirect.com/science/article/pii/S0257897210003701>.
- [8] M. Ashworth, M. Jacobs, and S. Davies, "Microstructure and property relationships in HIPped Stellite powders," *Powder Metallurgy*, vol. 42, no. 3, pp. 243–249, Mar. 1, 1999, ISSN: 0032-5899. DOI: [10.1179/003258999665585](https://doi.org/10.1179/003258999665585). Accessed: Apr. 3, 2025. [Online]. Available: <https://journals.sagepub.com/action/showAbstract>.
- [9] P. O. Bunch, M. P. Hartmann, and T. A. Bednarowicz, "Corrosion/Galling Resistant Hardfacing Materials for Offshore Production Valves," presented at the Offshore Technology Conference, OnePetro, May 1, 1989. DOI: [10.4043/6070-MS](https://doi.org/10.4043/6070-MS). Accessed: Apr. 1, 2025. [Online]. Available: <https://dx.doi.org/10.4043/6070-MS>.
- [10] J. Davis and A. Committee, *Nickel, Cobalt, and Their Alloys* (ASM Specialty Handbook). ASM International, 2000, ISBN: 978-0-87170-685-0. [Online]. Available: <https://books.google.ae/books?id=IePhmnbmRWkC>.
- [11] V. M. Desai, C. M. Rao, T. H. Kosel, and N. F. Fiore, "Effect of carbide size on the abrasion of cobalt-base powder metallurgy alloys," *Wear*, vol. 94, no. 1, pp. 89–101, Feb. 15, 1984, ISSN: 0043-1648. DOI: [10.1016/0043-1648\(84\)90168-6](https://doi.org/10.1016/0043-1648(84)90168-6). Accessed: Nov. 17, 2024. [Online]. Available: <https://www.sciencedirect.com/science/article/pii/0043164884901686>.
- [12] M. M. Ferozhkhan, K. G. Kumar, and R. Ravibharath, "Metallurgical Study of Stellite 6 Cladding on 309-16L Stainless Steel," *Arabian Journal for Science and Engineering*, vol. 42, no. 5, pp. 2067–2074, May 1, 2017, ISSN: 2191-4281. DOI: [10.1007/s13369-017-2457-7](https://doi.org/10.1007/s13369-017-2457-7). Accessed: Mar. 31, 2025. [Online]. Available: <https://doi.org/10.1007/s13369-017-2457-7>.
- [13] W. Pacquentin, P. Wident, J. Varlet, T. Cailloux, and H. Maskrot, "Temperature influence on the repair of a hardfacing coating using laser metal deposition and assessment of the repair innocuity," *Journal of Advanced Joining Processes*, vol. 11, p. 100 284, Jun. 1, 2025, ISSN: 2666-3309. DOI: [10.1016/j.jajp.2025.100284](https://doi.org/10.1016/j.jajp.2025.100284). Accessed: Mar. 31, 2025. [Online]. Available: <https://www.sciencedirect.com/science/article/pii/S2666330925000056>.
- [14] V. L. Ratia, D. Zhang, M. J. Carrington, J. L. Daure, D. G. McCartney, P. H. Shipway, and D. A. Stewart, "Comparison of the sliding wear behaviour of self-mated HIPed Stellite 3

- and Stellite 6 in a simulated PWR water environment,” *Wear*, 22nd International Conference on Wear of Materials, vol. 426–427, pp. 1222–1232, Apr. 30, 2019, ISSN: 0043-1648. DOI: [10.1016/j.wear.2019.01.116](https://doi.org/10.1016/j.wear.2019.01.116). Accessed: Jun. 30, 2024. [Online]. Available: <https://www.sciencedirect.com/science/article/pii/S004316481930211X>.
- [15] K. Zhang and L. Battiston, “Friction and wear characterization of some cobalt- and iron-based superalloys in zinc alloy baths,” *Wear*, vol. 252, no. 3, pp. 332–344, Feb. 1, 2002, ISSN: 0043-1648. DOI: [10.1016/S0043-1648\(01\)00889-4](https://doi.org/10.1016/S0043-1648(01)00889-4). Accessed: Apr. 1, 2025. [Online]. Available: <https://www.sciencedirect.com/science/article/pii/S0043164801008894>.
- [16] R. Ahmed, H. L. de Villiers Lovelock, and S. Davies, “Sliding wear of blended cobalt based alloys,” *Wear*, vol. 466–467, p. 203 533, Feb. 15, 2021, ISSN: 0043-1648. DOI: [10.1016/j.wear.2020.203533](https://doi.org/10.1016/j.wear.2020.203533). Accessed: Jul. 13, 2024. [Online]. Available: <https://www.sciencedirect.com/science/article/pii/S0043164820309923>.
- [17] P. Crook, “Cobalt-base alloys resist wear, corrosion, and heat,” *Cobalt-base alloys resist wear, corrosion, and heat*, vol. 145, no. 4, pp. 27–30, 1994, ISSN: 0882-7958.
- [18] B. A. Boeck, T. H. Sanders, V. Anand, A. J. Hickl, and P. Kumar, “Relationships Between Processing, Microstructure, and Tensile Properties of Co–Cr–Mo Alloy,” *Powder Metallurgy*, vol. 28, no. 2, pp. 97–104, Jan. 1, 1985, ISSN: 0032-5899. DOI: [10.1179/pom.1985.28.2.97](https://doi.org/10.1179/pom.1985.28.2.97). Accessed: May 12, 2025. [Online]. Available: <https://journals.sagepub.com/action/showAbstract>.
- [19] C. Zhang, H. Yin, J. Lv, Y. Du, Z. Tan, and Y. Liu, “Thermodynamic investigation of phase equilibria on the (W,Mo)C-(Co,Ni) cemented carbides,” *Calphad*, vol. 67, p. 101 664, Dec. 1, 2019, ISSN: 0364-5916. DOI: [10.1016/j.calphad.2019.101664](https://doi.org/10.1016/j.calphad.2019.101664). Accessed: May 18, 2025. [Online]. Available: <https://www.sciencedirect.com/science/article/pii/S0364591619301051>.
- [20] C. Zhang, Y. Peng, P. Zhou, and Y. Du, “Thermodynamic Modeling of the C-Co-Mo and C-Mo-Ni Ternary Systems,” *Journal of Phase Equilibria and Diffusion*, vol. 37, no. 4, pp. 423–437, Aug. 1, 2016, ISSN: 1863-7345. DOI: [10.1007/s11669-016-0471-1](https://doi.org/10.1007/s11669-016-0471-1). Accessed: May 18, 2025. [Online]. Available: <https://doi.org/10.1007/s11669-016-0471-1>.
- [21] H. Yu, R. Ahmed, H. d. V. Lovelock, and S. Davies, “Tribo-Mechanical Evaluations of Cobalt-Based (Stellite 4) Alloys Manufactured via HIPing and Casting,” 2007.
- [22] K. Ishida, “Intermetallic Compounds in Co-base Alloys–Phase Stability and Application to Superalloys,” *MRS Proceedings*, vol. 1128, 1128-U06–06, 2008, ISSN: 0272-9172, 1946–

4274. DOI: [10.1557/PROC-1128-U06-06](https://doi.org/10.1557/PROC-1128-U06-06). Accessed: May 18, 2025. [Online]. Available: <http://link.springer.com/10.1557/PROC-1128-U06-06>.
- [23] M. Zhao, H. Huang, T. Tang, and X. Li, “First-principles study on the preferential sites of Cr in Co_7W_6 ,” *Materials Research Express*, vol. 10, no. 3, p. 036 502, Mar. 1, 2023, ISSN: 2053-1591. DOI: [10.1088/2053-1591/aca5ef](https://doi.org/10.1088/2053-1591/aca5ef). Accessed: May 18, 2025. [Online]. Available: <https://iopscience.iop.org/article/10.1088/2053-1591/aca5ef>.
- [24] A. S. Kurlov and A. I. Gusev, “Phase equilibria in the W–C system and tungsten carbides,” *Russian Chemical Reviews*, vol. 75, no. 7, pp. 617–636, Jul. 31, 2006, ISSN: 0036-021X, 1468-4837. DOI: [10.1070/RC2006v075n07ABEH003606](https://doi.org/10.1070/RC2006v075n07ABEH003606). Accessed: May 11, 2025. [Online]. Available: <https://iopscience.iop.org/article/10.1070/RC2006v075n07ABEH003606>.
- [25] H. Tulhoff, “Carbides,” in *Ullmann’s Encyclopedia of Industrial Chemistry*, Wiley-VCH, Ed., 1st ed., Wiley, Jun. 15, 2000, ISBN: 978-3-527-30385-4 978-3-527-30673-2. DOI: [10.1002/14356007.a05_061](https://doi.org/10.1002/14356007.a05_061). Accessed: May 11, 2025. [Online]. Available: https://onlinelibrary.wiley.com/doi/10.1002/14356007.a05_061.
- [26] W. H. Jiang, X. D. Yao, H. R. Guan, and Z. Q. Hu, “Secondary M₆C Precipitation in a Cobalt–base Superalloy,” *Journal of Materials Science Letters*, vol. 18, no. 4, pp. 303–305, Feb. 1, 1999, ISSN: 1573-4811. DOI: [10.1023/A:1006627122234](https://doi.org/10.1023/A:1006627122234). Accessed: May 12, 2025. [Online]. Available: <https://doi.org/10.1023/A:1006627122234>.
- [27] Y. Li, Y. Gao, B. Xiao, T. Min, Y. Yang, S. Ma, and D. Yi, “The electronic, mechanical properties and theoretical hardness of chromium carbides by first-principles calculations,” *Journal of Alloys and Compounds*, vol. 509, no. 17, pp. 5242–5249, Apr. 28, 2011, ISSN: 0925-8388. DOI: [10.1016/j.jallcom.2011.02.009](https://doi.org/10.1016/j.jallcom.2011.02.009). Accessed: Jul. 14, 2024. [Online]. Available: <https://www.sciencedirect.com/science/article/pii/S0925838811003197>.
- [28] N. I. Medvedeva, D. C. Van Aken, and J. E. Medvedeva, “Stability of binary and ternary M₂₃C₆ carbides from first principles,” *Computational Materials Science*, vol. 96, pp. 159–164, Jan. 1, 2015, ISSN: 0927-0256. DOI: [10.1016/j.commatsci.2014.09.016](https://doi.org/10.1016/j.commatsci.2014.09.016). Accessed: Jul. 14, 2024. [Online]. Available: <https://www.sciencedirect.com/science/article/pii/S0927025614006272>.
- [29] M. Godec and D. A. Skobir Balantič, “Coarsening behaviour of M₂₃C₆ carbides in creep-resistant steel exposed to high temperatures,” *Scientific Reports*, vol. 6, no. 1, p. 29 734, Jul. 13, 2016, ISSN: 2045-2322. DOI: [10.1038/srep29734](https://doi.org/10.1038/srep29734). Accessed: Jul. 14, 2024. [Online]. Available: <https://www.nature.com/articles/srep29734>.

- [30] M. Mohammadnezhad, V. Javaheri, M. Shamanian, S. Rizaneh, and J. A. Szpunar, "Insight to the Microstructure Characterization of a HP Austenitic Heat Resistant Steel after Long-term Service Exposure,"
- [31] K. C. Antony, "Wear-Resistant Cobalt-Base Alloys," *JOM*, vol. 35, no. 2, pp. 52–60, Feb. 1, 1983, ISSN: 1543-1851. DOI: [10.1007/BF03338205](https://doi.org/10.1007/BF03338205). Accessed: Jul. 13, 2024. [Online]. Available: <https://doi.org/10.1007/BF03338205>.
- [32] F. Pettit and G. Meier, "Oxidation and Hot Corrosion of Superalloys," in *Superalloys 1984 (Fifth International Symposium)*, TMS, 1984, pp. 651–687. DOI: [10.7449/1984/Superalloys_1984_651_687](https://doi.org/10.7449/1984/Superalloys_1984_651_687). Accessed: May 17, 2025. [Online]. Available: http://www.tms.org/Superalloys/10.7449/1984/Superalloys_1984_651_687.pdf.
- [33] X. Z. Zhang, R. Liu, K. Y. Chen, and M. X. Yao, "Pitting Corrosion Characterization of Wrought Stellite Alloys in Green Death Solution with Immersion Test and Extreme Value Analysis Model," *Journal of Materials Engineering and Performance*, vol. 23, no. 5, pp. 1718–1725, May 1, 2014, ISSN: 1544-1024. DOI: [10.1007/s11665-014-0952-5](https://doi.org/10.1007/s11665-014-0952-5). Accessed: May 17, 2025. [Online]. Available: <https://doi.org/10.1007/s11665-014-0952-5>.
- [34] E. Lemaire and M. Le Calvar, "Evidence of tribocorrosion wear in pressurized water reactors," *Wear*, vol. 249, no. 5, pp. 338–344, Jun. 1, 2001, ISSN: 0043-1648. DOI: [10.1016/S0043-1648\(00\)00544-5](https://doi.org/10.1016/S0043-1648(00)00544-5). Accessed: May 17, 2025. [Online]. Available: <https://www.sciencedirect.com/science/article/pii/S0043164800005445>.
- [35] J. Di Martino, C. Rapin, P. Berthod, R. Podor, and P. Steinmetz, "Corrosion of metals and alloys in molten glasses. Part 2: Nickel and cobalt high chromium superalloys behaviour and protection," *Corrosion Science*, vol. 46, no. 8, pp. 1865–1881, Aug. 1, 2004, ISSN: 0010-938X. DOI: [10.1016/j.corsci.2003.10.025](https://doi.org/10.1016/j.corsci.2003.10.025). Accessed: May 17, 2025. [Online]. Available: <https://www.sciencedirect.com/science/article/pii/S0010938X03003081>.
- [36] A. Świetlicki, M. Szala, and M. Walczak, "Effects of Shot Peening and Cavitation Peening on Properties of Surface Layer of Metallic Materials—A Short Review," *Materials*, vol. 15, no. 7, p. 2476, 7 Jan. 2022, ISSN: 1996-1944. DOI: [10.3390/ma15072476](https://doi.org/10.3390/ma15072476). Accessed: May 12, 2025. [Online]. Available: <https://www.mdpi.com/1996-1944/15/7/2476>.
- [37] D. A. Woodford, "Cavitation-erosion-induced phase transformations in alloys," *Metallurgical Transactions*, vol. 3, no. 5, pp. 1137–1145, May 1972, ISSN: 0026-086X, 2379-0083. DOI: [10.1007/BF02642445](https://doi.org/10.1007/BF02642445). Accessed: May 18, 2025. [Online]. Available: <https://link.springer.com/10.1007/BF02642445>.

- [38] R. Ahmed, V. Kumar, N. H. Faisal, M. Marri, and S. Davies, "Influence of Alloy Composition on the Tribomechanical Properties of 50% Blend of CoCrWMoCFeNiSiMn (Stellite 1) and CoCrMoCFeNiSiMn (Stellite 21) Alloys," *Journal of Materials Engineering and Performance*, Mar. 24, 2025, ISSN: 1544-1024. DOI: [10.1007/s11665-025-11034-7](https://doi.org/10.1007/s11665-025-11034-7). Accessed: Apr. 13, 2025. [Online]. Available: <https://doi.org/10.1007/s11665-025-11034-7>.
- [39] R. P. Reed and R. E. Schramm, "Relationship between stacking-fault energy and x-ray measurements of stacking-fault probability and microstrain," *Journal of Applied Physics*, vol. 45, no. 11, pp. 4705–4711, Nov. 1, 1974, ISSN: 0021-8979. DOI: [10.1063/1.1663122](https://doi.org/10.1063/1.1663122). Accessed: May 18, 2025. [Online]. Available: <https://doi.org/10.1063/1.1663122>.
- [40] N. S. McIntyre, D. Zetaruk, and E. V. Murphy, "X-Ray photoelectron spectroscopic study of the aqueous oxidation of stellite-6 alloy," *Surface and Interface Analysis*, vol. 1, no. 4, pp. 105–110, 1979, ISSN: 1096-9918. DOI: [10.1002/sia.740010402](https://doi.org/10.1002/sia.740010402). Accessed: May 11, 2025. [Online]. Available: <https://onlinelibrary.wiley.com/doi/abs/10.1002/sia.740010402>.
- [41] Z. Česánek, J. Schubert, Š. Houdková, O. Bláhová, and M. Prantnerová, "Deterioration of Local Mechanical Properties of HVOF-Sprayed Stellite 6 after Exposure to High-Temperature Corrosion," *Key Engineering Materials*, vol. 662, pp. 115–118, 2015, ISSN: 1662-9795. DOI: [10.4028/www.scientific.net/KEM.662.115](https://doi.org/10.4028/www.scientific.net/KEM.662.115). Accessed: May 11, 2025. [Online]. Available: <https://www.scientific.net/KEM.662.115>.
- [42] C. J. Heathcock, A. Ball, and B. E. Protheroe, "Cavitation erosion of cobalt-based Stellite® alloys, cemented carbides and surface-treated low alloy steels," *Wear*, vol. 74, no. 1, pp. 11–26, Dec. 8, 1981, ISSN: 0043-1648. DOI: [10.1016/0043-1648\(81\)90191-5](https://doi.org/10.1016/0043-1648(81)90191-5). Accessed: Feb. 5, 2025. [Online]. Available: <https://www.sciencedirect.com/science/article/pii/0043164881901915>.
- [43] "Cavitation Erosion," in *Fundamentals of Cavitation*, J.-P. Franc and J.-M. Michel, Eds., Dordrecht: Springer Netherlands, 2005, pp. 265–291, ISBN: 978-1-4020-2233-3. DOI: [10.1007/1-4020-2233-6_12](https://doi.org/10.1007/1-4020-2233-6_12). Accessed: Apr. 13, 2025. [Online]. Available: https://doi.org/10.1007/1-4020-2233-6_12.
- [44] S. Romo, J. Santa, J. Giraldo, and A. Toro, "Cavitation and high-velocity slurry erosion resistance of welded Stellite 6 alloy," *Tribology International*, vol. 47, pp. 16–24, 2012, ISSN: 0301679X (ISSN). DOI: [10.1016/j.triboint.2011.10.003](https://doi.org/10.1016/j.triboint.2011.10.003). [Online]. Available: <https://www.scopus.com/inward/record.uri?eid=2-s2.0-84856240362&doi=10.1016%2fj.triboint.2011.10.003&partnerID=40&md5=77bc5b529937543083c683cc6f5d689d>.

- [45] M. T. Gevari, T. Abbasiasl, S. Niazi, M. Ghorbani, and A. Koşar, “Direct and indirect thermal applications of hydrodynamic and acoustic cavitation: A review,” *Applied Thermal Engineering*, vol. 171, p. 115 065, May 5, 2020, ISSN: 1359-4311. DOI: [10.1016/j.applthermaleng.2020.115065](https://doi.org/10.1016/j.applthermaleng.2020.115065). Accessed: Apr. 13, 2025. [Online]. Available: <https://www.sciencedirect.com/science/article/pii/S135943111937766X>.
- [46] Z. Huang, B. Wang, F. Liu, M. Song, S. Ni, and S. Liu, “Microstructure evolution, martensite transformation and mechanical properties of heat treated Co-Cr-Mo-W alloys by selective laser melting,” *International Journal of Refractory Metals and Hard Materials*, vol. 113, p. 106 170, Jun. 1, 2023, ISSN: 0263-4368. DOI: [10.1016/j.ijrmhm.2023.106170](https://doi.org/10.1016/j.ijrmhm.2023.106170). Accessed: Apr. 13, 2025. [Online]. Available: <https://www.sciencedirect.com/science/article/pii/S0263436823000707>.
- [47] H. M. Tawancy, V. R. Ishwar, and B. E. Lewis, “On the fcc \rightarrow hcp transformation in a cobalt-base superalloy (Haynes alloy No. 25),” *Journal of Materials Science Letters*, vol. 5, no. 3, pp. 337–341, Mar. 1, 1986, ISSN: 1573-4811. DOI: [10.1007/BF01748098](https://doi.org/10.1007/BF01748098). Accessed: Apr. 13, 2025. [Online]. Available: <https://doi.org/10.1007/BF01748098>.
- [48] H. Yu, R. Ahmed, and H. de Villiers Lovelock, “A Comparison of the Tribo-Mechanical Properties of a Wear Resistant Cobalt-Based Alloy Produced by Different Manufacturing Processes,” *Journal of Tribology*, vol. 129, no. 3, pp. 586–594, Jan. 9, 2007, ISSN: 0742-4787. DOI: [10.1115/1.2736450](https://doi.org/10.1115/1.2736450). Accessed: Nov. 17, 2024. [Online]. Available: <https://doi.org/10.1115/1.2736450>.
- [49] V. Stoica, R. Ahmed, and T. Itsukaichi, “Influence of heat-treatment on the sliding wear of thermal spray cermet coatings,” *Surface and Coatings Technology*, vol. 199, no. 1, pp. 7–21, 2005, ISSN: 02578972 (ISSN). DOI: [10.1016/j.surfcoat.2005.03.026](https://doi.org/10.1016/j.surfcoat.2005.03.026). [Online]. Available: <https://www.scopus.com/inward/record.uri?eid=2-s2.0-21844464044&doi=10.1016%2fj.surfcoat.2005.03.026&partnerID=40&md5=6ad736723e828d39edf4a37c5975d2dc>.
- [50] R. Ahmed, H. L. de Villiers Lovelock, S. Davies, and N. H. Faisal, “Influence of Re-HIPing on the structure–property relationships of cobalt-based alloys,” *Tribology International*, vol. 57, pp. 8–21, Jan. 1, 2013, ISSN: 0301-679X. DOI: [10.1016/j.triboint.2012.06.025](https://doi.org/10.1016/j.triboint.2012.06.025). Accessed: Jun. 30, 2024. [Online]. Available: <https://www.sciencedirect.com/science/article/pii/S0301679X12002241>.
- [51] H. Yu, R. Ahmed, H. d. V. Lovelock, and S. Davies, “Influence of Manufacturing Process and Alloying Element Content on the Tribomechanical Properties of Cobalt-Based Alloys,” *Journal of Tribology*, vol. 131, no. 011601, Dec. 4, 2008, ISSN: 0742-4787. DOI: [10.1115/](https://doi.org/10.1115/)

- 1.2991122. Accessed: May 1, 2025. [Online]. Available: <https://doi.org/10.1115/1.2991122>.
- [52] M. Szala, D. Chocyk, A. Skic, M. Kamiński, W. Macek, and M. Turek, “Effect of nitrogen ion implantation on the cavitation erosion resistance and cobalt-based solid solution phase transformations of HIPed stellite 6,” *Materials*, vol. 14, no. 9, 2021, ISSN: 19961944 (ISSN). DOI: [10.3390/ma14092324](https://doi.org/10.3390/ma14092324). [Online]. Available: <https://www.scopus.com/inward/record.uri?eid=2-s2.0-85105941706&doi=10.3390%2fma14092324&partnerID=40&md5=4c846be7d06977d42697c88c326e5923>.
- [53] A. Thiruvengadam, “Theory of erosion,” *Proc. 2nd Meersburg Conf. on Rain Erosion and Allied Phenomena*, vol. 2, p. 53, Mar. 1, 1967.